

Article

Experimental Study on the Gelling Properties of Nano-Silica Sol and Its Spontaneous Imbibition Grouting Mudstone

Yiming Zhao ¹, Zhe Xiang ^{1,*} , Nong Zhang ^{1,2}  and Jingchen Dai ¹

¹ Key Laboratory of Deep Coal Resource Mining of the Ministry of Education, School of Mines, China University of Mining and Technology, Xuzhou 221116, China; zhaoyiming@cumt.edu.cn (Y.Z.); zhangnong@cumt.edu.cn (N.Z.); ts23020010a31tm@cumt.edu.cn (J.D.)

² School of Civil Engineering, Xuzhou University of Technology, Xuzhou 221000, China

* Correspondence: xiangzhe0@cumt.edu.cn

Abstract: The low-permeability argillaceous rock mass is an unfavorable geological body commonly found in the construction process of underground engineering conditions such as roadways and tunnels. Due to the compact structure and low permeability of the rock mass, grouting with conventional materials cannot effectively seal the micro-cracks of the rock mass. Based on the low efficiency of high-pressure grouting of nano-silica sol, this paper preliminarily explores the regularities and mechanism of grouting and pore sealing of low-permeability rock mass under the action of silica sol imbibition from the aspects of gelling properties of silica sol, core pore structure, imbibition law, and pore sealing characteristics. The results show the following: (1) The increase in particle size during the gel process reduced the injectability and wettability of the silica sol. The imbibition properties of silica sol were time-varying, and the deterioration inflection points of injectability and wettability appeared at 10 h and 9 h, respectively. (2) Catalyst, temperature, gel process, and rock mass permeability will affect the law of core imbibition, and the injectability and capillary force of the grouting material and rock mass will jointly affect the imbibition process of silica sol. (3) Silica sol imbibition changed the pore size distribution of the core, the pore volume above 50 nm decreased, and the pore volume below 50 nm increased. Silica sol has multiple effects such as filling, adsorption, and percolation in the imbibition process of the micro-pores of rock mass, and the adsorption and percolation of silica are related to the nano micro-pores.

Keywords: low-permeability rock mass; silica sol; imbibition grouting; pore structure



Citation: Zhao, Y.; Xiang, Z.; Zhang, N.; Dai, J. Experimental Study on the Gelling Properties of Nano-Silica Sol and Its Spontaneous Imbibition Grouting Mudstone. *Processes* **2024**, *12*, 983. <https://doi.org/10.3390/pr12050983>

Academic Editor: Masoud Soroush

Received: 17 April 2024

Revised: 7 May 2024

Accepted: 10 May 2024

Published: 12 May 2024



Copyright: © 2024 by the authors. Licensee MDPI, Basel, Switzerland. This article is an open access article distributed under the terms and conditions of the Creative Commons Attribution (CC BY) license (<https://creativecommons.org/licenses/by/4.0/>).

1. Introduction

Low-permeability unfavorable geological bodies such as mudstone, argillaceous inter-layer, and mud-bearing fracture zone are commonly found in underground engineering in China [1,2]. Their occurrence state and pore structure characteristics are closely related to engineering construction, which, in many cases, has a significant impact on the safety and stability of engineering structures [3,4]. The argillaceous rock mass contains a large proportion of clay minerals, and its physical properties are easily affected by changes in the water environment [5,6]. It is almost impossible to avoid the influence of groundwater in underground engineering such as mine roadways and tunnels, especially for argillaceous soft rock roadways in coal mines. Water erosion on argillaceous rock mass and progressive failure of the supporting structure is prominent. The argillization of argillaceous soft rocks by fissure water leads to the weakening or failure of the encapsulation structure, which is often one of the important incentives for the failure of bolt and cable and roof fall in argillaceous roadway [7,8]. The grouting method is an effective technique to seal the fissure water of surrounding rock in underground engineering construction. The character of surrounding rock can be fundamentally improved by grouting to modify and consolidate argillaceous soft rock, sealing the cracks in surrounding rock, and preventing the immersion of fissure water and argillization of surrounding rock. A large number of studies

and engineering practices have shown that the grouting modification of low-permeability argillaceous rock mass is closely related to the injectability of grouting material [9,10]. The minimum grouting crack width of conventional cement and superfine cement is 0.01 mm, which can only seal the macroscopic crack of rock mass [11,12]. However, the plugging of micro-pores (0.3–5 μm [13,14]) that play a major role in groundwater seepage is almost ineffective. This means that the inorganic grouting material represented by cement grout has a poor modification and reinforcement effect on argillaceous soft rock. However, chemical grouting materials with high injectability such as polyurethane and epoxy resin are limited to use in some underground engineering due to their toxicity, self-heating, and cost [15–17]. In short, as controlling the large deformation and failure of argillaceous rock mass remains a problem that cannot be avoided, attention should be paid to address the grouting sealing and reinforcement of micro-pores of argillaceous rock mass in underground engineering conditions.

The need for sealing and consolidation of micro-pores has led to an international surge in the amount of research on nano grouting materials and grouting technology in geotechnical engineering applications. In recent years, a new nano grouting material—silica sol—has been tried in the field of anti-seepage reinforcement of underground engineering. Funehag et al. [18–20] took the lead in using silica sol to seal rock micro-cracks in a hard rock tunnel, effectively improving the hydraulic conductivity of tunnel surrounding rock as low as 3×10^{-9} m/s. Wang et al. [21] used high-performance concrete wet-spraying and silica sol grouting technology to effectively seal the pore water in the rock formation, and they solved the problem of water gushing on the inclined shaft wall of Xiaojihan coal mine. Based on the composite grouting technology of superfine cement and silica sol, Holter and Hogestad [22] proposed an advanced pre-grouting construction method for immersed tunnels and other underground engineering conditions. Date et al. [23] used silica sol and superfine cement to grout the bulkhead area of the Kitame Tunnel in Japan to seal the water, and finally they formed an effective grouting impervious area. To sum up, compared with traditional cement grout and chemical grout, nano silica sol is characterized by its non-toxic nature and environmental protection, small particle size, strong permeability, dense gel, and stable chemical properties.

Due to the advantages of particle size, silica sol can theoretically meet the requirements of the injectability of nano micro-pores in a low-permeability rock mass, but the grouting effect is dismal in the initial research stage due to inappropriate grouting methods. Pan et al. [24,25] carried out a high-pressure grouting test of silica sol on loose coal bodies with different fragmentation degrees. It was found that during the high-pressure grouting process of silica sol, the grouting port would create the filter cake effect due to the continuous growth of the gel particle size, and then it would reduce the grouting effect. Guo et al. [26] analyzed the grouting seepage law of silica sol under the dual influence of pressure and permeability by nuclear magnetic resonance (NMR). The results show that the critical permeability of silica sol grouted into the rock mass at high pressure is about 40.42 mD. The low-permeability core of 1 mD cannot be grouted by 3 MPa high-pressure grouting (see Figure 1a for the NMR information of the 1–100 mD permeability cores after grouting). The above research results show that the feasibility of high-pressure grouting of silica sol for low-permeability rock is low, even if the particle size is in the nanometer scale.

Spontaneous imbibition is a hydrodynamic phenomenon commonly found in the micro-pore structure of rock, soil, cement, electrodes, and other materials. It refers to the multiphase flow process of wetting phase fluid spontaneously entering into porous media and replacing the non-wetting phase fluid inside [27,28]. Its driving force comes from the capillary pressure generated by the micro-pores. It is generally believed [29] that the capillary imbibition height and rising rate of porous media are inversely related to the pore diameter. The smaller the pores of the porous medium, the greater the capillary imbibition height. The research results of the imbibition theory of chemical grouting [30] show that imbibition is another spontaneous infiltration force besides pressure infiltration and is an important internal driving force for the migration and flow of nano-scale grouting

material in the micro-cracks of rock mass. Through low-pressure imbibition, epoxy grouting material can realize the grouting consolidation of intergranular pores of low-permeability argillaceous rock mass, and the minimum permeability coefficient of grouting rock is $k \approx 10^{-8}$ cm/s [31]. The median particle size of the silica sol is on the nanometer scale, the specific surface area is large, the wettability to the rock and soil medium is good, and the imbibition potential is outstanding. Meanwhile, the dominant pore size of low-permeability rock mass is in the micro-nano scale, the micro pores are developed, and the surface free energy is higher. The stronger capillary force will make the spontaneous imbibition of silica sol more obvious. Based on the above cognition, the spontaneous imbibition test of silica sol was carried out in the early stage of the test. Figure 1b shows the imbibition curve and physical picture of 1 mD artificial core. The imbibition result indicates that the silica sol can be grouted into the 1 mD rock body by spontaneous imbibition. It also shows that it is feasible to grout low-permeability rock mass by spontaneous imbibition of silica sol and takes advantage of the gelling properties to seal micro-nano pores.

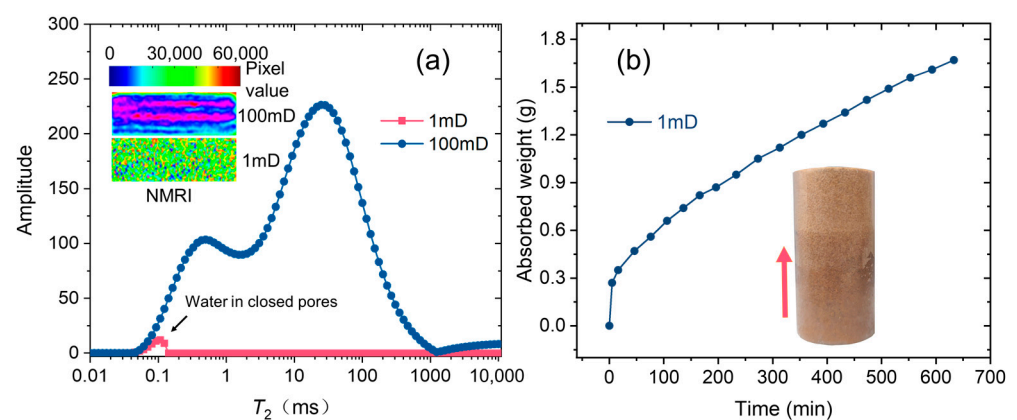


Figure 1. Characteristics of silica sol grouting in the low-permeability rock mass. (a) NMR information of high-pressure grouting of 1–100 mD cores; (b) the imbibition curve of 1 mD artificial core to silica sol and the physical picture after imbibition.

In allusion to the imbibition phenomenon of silica sol and low-permeability rock mass under capillary force and the feasibility of grouting through imbibition, this study attempts to explore the law and mechanism of grouting and closed pores of low-permeability rock mass under the imbibition of silica sol. However, the imbibition of silica sol and low-permeability rock mass is a complex physical and chemical reaction, one that involves many complex processes such as capillary traction of porous media, flow, adsorption, filtration, and solidification of silica sol. Therefore, it is necessary to consider the material properties of the silica sol, the pore structure of the rock mass, and the characteristics of the solid–liquid interface and so on. In this paper, a variety of modern test and analysis methods are used on this basis to finely explore the physical property changes in the gel process of silica sol, the law of imbibition grouting under various influencing factors, and the law of rock pore closure of imbibition grouting. The time-varying of the injectability, wettability, and imbibition potential of the grouting material in the gel process was analyzed on the basis of the change of particle size distribution and contact angle of silica sol. The internal mechanism of imbibition grouting and pore closure of low-permeability rock mass and silica sol was analyzed by NMR and nitrogen adsorption. Finally, the limitations of high-pressure grouting and the engineering significance and application prospects of the imbibition grouting of silica sol are discussed.

2. Experimental Design

2.1. Experimental Materials and Equipment

(1) Nano Silica Sol

Silica sol, also known as silicic acid sol, is a milky white or light blue sol liquid. It is a stable dispersion system of amorphous SiO₂ colloidal particles in an aqueous solution, and the size of the colloidal particles is 1~100 nm. The internal structure of the silica sol micelle is a three-dimensional network structure linked by siloxane bonds [32,33]. The center of the particle is the micelle, which is a polymer consisting of silica molecules [34]. A large number of hydroxyl groups formed on the surface of the micelle, together with alkali metal counterions in the colloidal solution, jointly form a diffuse double layer. The surface of the colloidal particles has the same charge, and the electrostatic repulsion between them plays a decisive role in the stability of the colloidal silica [35].

The nano silica sol for the test is an ordinary commercial silica sol provided by Shandong YinFeng Nano New Materials Co., Ltd., Qingdao, China. Table 1 shows its basic properties. According to previous experimental studies, 10% NaCl solution as a catalyst can make the gel process of silica sol more stable and has certain advantages in terms of efficiency and cost. The catalyst was a self-made NaCl solution with a mass fraction of 10%.

Table 1. Properties of silica sol.

pH	Density (g/cm ³)	Average Particle Size (nm)	SiO ₂ Concentration (%)	Na ₂ O Concentration (%)
9.55	1.203	9.6	30%	0.31

Note: Na₂O provides alkali metal counterions for maintaining the stability of colloidal solution.

(2) Artificial core

In view of the physical properties of natural mudstone, i.e., mudding when encountering water (pore collapse), natural mudstone cannot obtain accurate permeability by permeability screening. Therefore, artificial rocks are used to replace natural mudstones in order to ensure the repeatability of the imbibition process. The artificial core provided by Beijing HuaRuiXinCheng Science and Technology Co., Ltd. (Beijing, China), is mainly composed of dolomite, clay, and epoxy resin, and it is pressed into a cylindrical core of $\varnothing 25 \times 50$ mm at high temperature. With the rock mass permeability classification method [36], low-permeability rock mass refers to the permeability $k < 50$ mD. Low-permeability cores of 0.1 mD, 1 mD, 20 mD, and 40 mD were selected by the permeability test, with an error no more than $\pm 10\%$. See Table 2 for the physical parameters of the partial artificial cores.

Table 2. Physical parameters of artificial cores.

Permeability (mD)	Measured Permeability (mD)	Height (mm)	Diameter (mm)	Porosity (%)
0.1	0.11	49.66	25.4	4.21
1	1.08	50.44	24.88	6.19
20	21.41	50.35	25.27	8.71
40	39.13	50.14	25.34	10.11

(3) Experimental equipment

The experimental equipment is shown in Table 3.

Table 3. List of experimental instruments.

Experimental Equipment	Model Number	Function and Testing Content
Nanoparticle size analyzer	Zetasizer Nano ZSE	Measurement of particle size distribution in the process of silica sol gel
Contact angle analyzer	DSA100	Test the contact angle between silica sol and mudstone to characterize wettability
Specific surface area and pore size analyzer	TriStarII3020	Test the pore size distribution of rocks before and after silica sol imbibition
Thermostatic water bath	HH-6	Maintain consistent temperature of silica sol during the testing process
Low-field NMR	MacroMR12-150H-I	Test the pore size distribution at the macro and micro scales of rock cores
Vacuum pressure saturation device Dehydrator	ZYB-II DHG-9003	Perform saturation water treatment on the rock core Drying the core to calculate porosity

2.2. Test Method

2.2.1. Gelling Properties Test of Silica Sol

(1) Gel time test of silica sol

The inverted cup method was used to test the change rule of the gel time of the mixed silica sol (volume ratio of 10:1) at different catalyst ratios and temperatures [26]. The catalyst was tested at room temperature (25 °C), and the thermostat water bath cauldron was used to keep the silica sol temperature constant.

(2) Particle size distribution test of silica sol

Silica sol and catalyst were mixed in a specific proportion. After a specific time for gelling, part of the silica sol was taken out, and the mass fraction of SiO₂ was diluted to 1% with deionized water and then was well stirred. The particle size distribution of the sample was measured by a nano-laser particle size analyzer.

(3) Contact angle test

The low-permeability core was cut into 8 mm thin slices, and the surface of the rock sample was polished with 600-mesh fine sandpaper to eliminate the uneven rock surface. A contact angle analyzer was used to measure the contact angle (CA) of silica sol with different gel time to the low-permeability rock mass [24]. The droplet volume was set as 2 µL. Each sample was tested three times at different positions on the rock surface, with the left and right angles of the droplet counted, and the average value then taken.

2.2.2. Test of the Imbibition Law of Silica Sol

The imbibition device is shown in Figure 2. The cores were dried and encapsulated with a heat shrink tube before the imbibition test. The silica sol was mixed with the catalyst by a specific proportion (or just adding the silica sol), and the mixture was quickly poured into the container. All rock cores were put in and timed, taken out at certain intervals to have the excess grout wiped from the surface of the cores, and weighed until the grout lost fluidity by retest.

According to the above experimental procedure, cores with permeability of 1 mD were used to test the imbibition curves at different temperatures with/without catalyst addition. After adding catalyst, the imbibition curves were tested at different gel times. Finally, the imbibition curves for four permeability cores (0.1 mD, 1 mD, 20 mD, 40 mD) were tested. In the experiment, a thermostat water bath cauldron was used to keep the temperature of the grouting material.

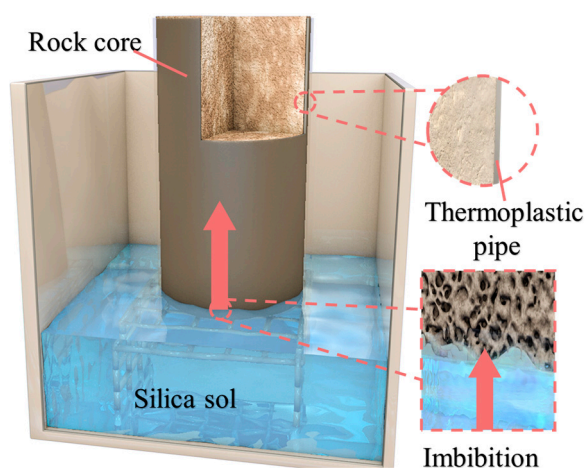


Figure 2. Schematic diagram of the imbibition device.

2.2.3. Sealing Test of Rock Micro-Cracks by Imbibition Grouting

(1) Macroscopic porosity test

The porosity changes of cores with different permeability before and after imbibition were tested by the vacuum saturation method [27] so as to represent the macroscopic overall pore closure characteristics of rock mass in the imbibition process. We calculated the porosity of the rock mass by dividing the weight difference of the core sample before and after saturation with water by the weight of the saturated water core.

(2) Microscopic pore size distribution test

The NMR test will affect the test results on account of the H atoms abundant in the silica sol. Micro-nano pores of artificial cores will be destroyed by the mercury injection method as artificial cores have less structural strength than natural cores. Due to the nano-scale silica particle size of silica sol, the specific surface area and pore size distribution analyzer were used to test the change rule of the pore size distribution of the samples before and after imbibition so as to represent the sealing effect of silica on the micro-nano pore of artificial rock cores. Moreover, microscopic pore size distribution is not affected by the macroscopic pores and cracks of the samples, so the cores were broken into 2–3 mm small rocks for testing before and after imbibition.

3. Results and Discussion

3.1. Gelling Properties of Silica Sol

3.1.1. Gel Time of Silica Sol

The appropriate amount of alkali metal counterions in the silica sol can balance the charge of the system and play a stable role on the colloid [37]. When the concentration of alkali metal ions exceeds a limit, it will play an opposite role in promoting colloidal aggregation [38]. Due to a high salt concentration, the silica nano micelle double-layer collapsed with decreased stabilizing repulsive force, leading to the dehydration condensation reaction of silicon hydroxyl on the surface of different silica sol particles [15]. This makes the silica sol monomer particles cross-linked, and thus the stability of the colloidal silica is gradually reduced. The interlaced network structure is formed by the cross-linking of silica sol polymer or silica sol particles, and finally a dense solid silica gel with stable chemical properties throughout the silica sol space is formed.

Based on the previous content, the dehydration condensation reaction between silica sol particles occurs instantaneously, but due to the large amount of colloidal silica particles, it takes some time to form a gel network structure. This provides operable time for the engineering use of silica sol. See Figure 3 for the gel time of silica sol with different amounts of catalyst addition tested by the “inverted cup method”. The figure shows that with the increase in NaCl concentration, the aggregation rate of silica nanoparticles increased, the

gel time was significantly shortened, and the amount of catalyst added and the gel time were distributed exponentially. At the same time, because the gel time after mixing was determined for a specific proportion of silica sol and coagulant, the error here was almost negligible. Therefore, the gelation process of the silica sol can be controlled by controlling the addition ratio of the catalyst. In order to reduce the influence of test time on the test results, the volume ratio of silica sol and catalyst was 10:1 and the gel time was 10 h and 43 min in this experiment.

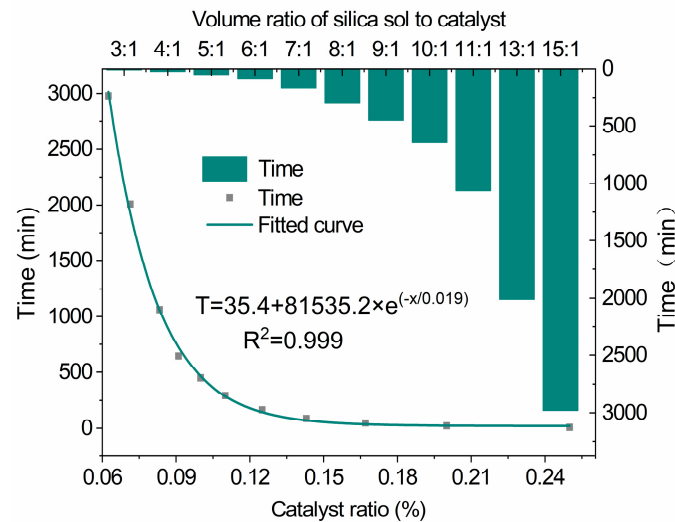


Figure 3. Gel time of silica sol.

3.1.2. Time-Varying Characteristics of Injectability of Silica Sol in the Gel Process

The ratio of the geometric parameters of rock medium permeability to the particle size of the grouting material is the main content of the research on the injectability of the low-permeability rock mass. According to the principle of injectability of fractured media [39,40], whether the injected medium is pore-shaped or fissured, the pore diameter and fissure width should be more than three times larger than the diameter of the coarsest particle of the grouting material. Therefore, when the pore characteristics of the rock mass are determined, the injectability of the rock mass is mainly affected by the particle size and distribution characteristics of the grouting material. In the gelation process of silica sol, the aggregation of silica micelles will inevitably change the particle size distribution of silica sol, thus affecting the injectability of silica sol.

Figure 4 is the particle size distribution curve of silica sol with different gel times. According to the particle size test results, the particle size distribution curve showed a unimodal distribution before the catalyst was added, and the median particle size was 9.6 nm, indicating that the silica sol was uniformly dispersed in water, without particle aggregation, and the initial injectability was the best. After adding the catalyst, the particle size distribution curve changed from a single peak to dual peak. With the increase in gel time, the median particle size of the first peak and the second peak gradually increased, but the area of the first peak gradually decreased, and the area of the second peak gradually increased. The third peak appeared until the eighth hour, and the area of the third peak continued to increase, indicating that with the catalyst, the silica nano-scale micelles inside the silica sol were continuously aggregated under the traction of the Coulomb force, and the particle size distribution of the silica sol gradually shifted to a large size, and the micro-sized micelles were formed in the later stage of gelation. This will reduce the permeability of the silica sol in the micro-pore throat of the rock mass, thereby affecting the injectability of the silica sol.

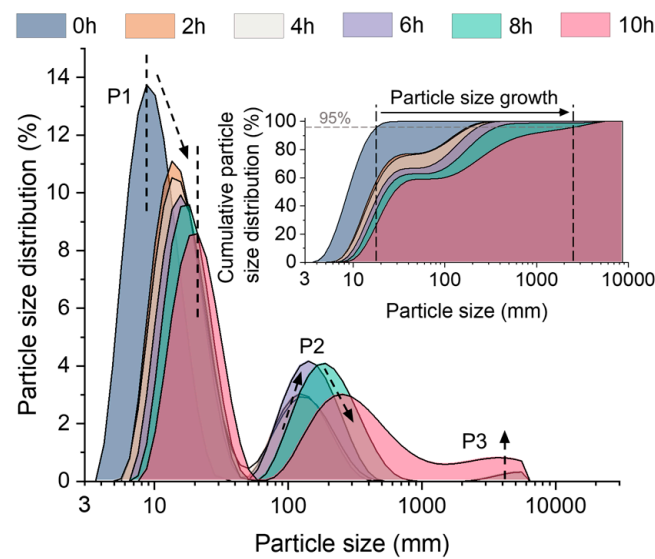


Figure 4. Particle size distribution and cumulative particle size distribution.

In order to further accurately characterize the effect of particle size growth on the injectability of silica sol, cement and superfine cement [41] was quantitatively analyzed and compared according to the injectability principle of fractured medium, together with the cumulative pore size distribution of typical low-permeability mudstone [42] (mercury injection method, $k = 5.87$ mD) and the cumulative particle size distribution law of silica sol. The results are shown in Figure 5 and Table 4. D_{95} is the corresponding particle size of the grouting material, accounting for 95% of the cumulative particle size distribution curve. R_{3d95} is the ratio of the cumulative porosity above the corresponding porosity value of the $3d_{95}$ particle size on the cumulative pore size distribution curve of the mudstone to the total porosity of the mudstone. It indicates the proportion of pores in the rock body that can allow the passage of silica sol of this particle size, which is used to show the injectability of the grouting material.

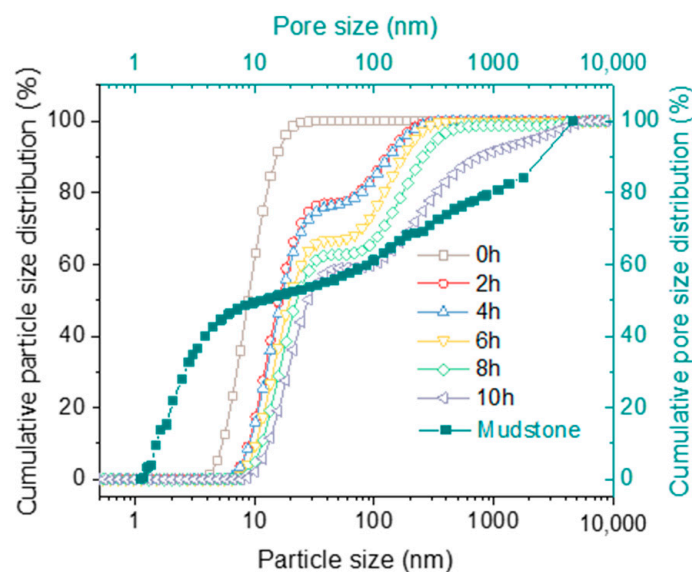


Figure 5. Comparison of the injectability of silica sol.

Table 4 shows that the d_{95} of the silica sol was 17.59 nm before adding the catalyst, the corresponding $R_{3d_{95}}$ was 51.38%, and the injectability was maximum at this time. Two hours after adding the catalyst, the d_{95} suddenly increased to 168 nm, and the corresponding

R^{3d95} dropped to 44.53%. With the increase in gel time, d_{95} gradually increased and R^{3d95} decreased slowly. At the 10th hour, the mutation point of d_{95} and R^{3d95} appeared, d_{95} suddenly increased to 2366 nm, and the corresponding R^{3d95} decreased to 29.41%, indicating that only 29.41% of the pores in the mudstone can allow the passage of silica sol, and that the injectability of silica sol was greatly reduced.

Table 4. Change rule of injectability.

Category		d_{95}/nm	$3d_{95}/\text{nm}$	$R^{3d_{95}}/\%$
Silica sol	0 h	17.59	52.77	51.38
	2 h	168	504	44.53
	4 h	178	534	44.36
	6 h	219	657	43.56
	8 h	341	1023	41.47
	10 h	2366	7098	29.41
Micro-fine cement		16,262	48,787	19.2
Ordinary cement		58,561	175,684	9.18

For ordinary cement and superfine cement, the d_{95} were 58561 nm and 16262 nm, and the corresponding $R^{3d_{95}}$ were 9.18% and 19.2%, respectively. Due to the large particle size of ordinary cement and superfine cement, their injectability to mudstone was much smaller than that of silica sol. The injectability of silica sol without catalyst was 5.6 times and 2.67 times that of ordinary cement and superfine cement, respectively, while the injectability of silica sol was 3.2 times and 1.53 times higher than that of ordinary cement and superfine cement, respectively, when the catalyst gel was added for 10 h. It showed that even if the particle size of silica sol increased significantly in the late gelation stage, the injectability was still better than that of cement grout and superfine cement, indicating that silica sol has good injectability in the gel process.

3.1.3. Time-Varying Characteristics of Wettability of Silica Sol in the Gel Process

In the solid-grout coexistence system, the grout can be imbibed spontaneously as long as the solid has affinity [43,44]. The CA of the silica sol and the rock surface reflects the wettability of the grouting material to the injected medium. If $CA > 90^\circ$, the grouting material is the non-wetting phase of the injected medium, and the injected medium has no affinity. If $CA < 90^\circ$, the grouting material is the wetting phase, and the injected medium has affinity and imbibition potential; moreover, the smaller the contact angle, the greater the affinity and osmotic potential. Table 5 shows the variation of the contact angle between silica sol and low-permeability rock with gel time.

Table 5. Contact angle of silica sol at different times.

Time/h	Right CA/ $^\circ$	Left CA/ $^\circ$	Average CA/ $^\circ$	Photo	Time/h	Right CA/ $^\circ$	Left CA/ $^\circ$	Average CA/ $^\circ$	Photo
1	26.27	27.19	28.21		3	33.89	37.15	37.80	
	33.69	32.20				41.12	39.13		
	22.40	27.50				37.15	38.35		
5	47.23	45.58	51.35		7	67.20	63.44	61.51	
	60.44	63.44				74.36	59.49		
	47.44	43.96				57.38	47.16		
8	65.94	74.44	63.44		9	82.28	76.43	84.02	
	60.46	55.01				83.93	82.19		
	61.03	63.75				91.17	88.09		
9.5	91.17	90.20	94.06		10	100.71	98.62	99.74	
	96.01	96.23				102.89	95.10		
	97.13	93.63				100.01	101.11		

When the gel time was 1h, the minimum CA was 28.21° , and the affinity of the grouting material was the best. As the gel time increased, the CA of the silica sol gradually increased, and the affinity of the grouting material gradually decreased. Within 1–9 h, the CA of the silica sols were all less than 90° , indicating that the injected medium had affinity during the 9h gel time. At this time, when the injected medium was in a dry or unsaturated state, the silica sol was able to automatically penetrate into the injected medium. The CA exceeded 90° in 9~9.5 h, and the grouting material changed from wetting to non-wetting. After 9.5 h, the grouting material was unable to spread on the surface of the medium, and the injected medium did not have affinity. At this time, the silica sol was unable to automatically penetrate into the injected medium by capillary force, indicating that the micelle aggregation-the growth of particle size in the gelation process of silica sol had a significant effect on the wettability of the grout, and that the grouting material would not have the imbibition ability in the later stage of gelation. For the silica sol with a ratio of 10:1, the time of indicating the imbibition feature was within 9 h after gelation.

However, in the detailed construction process, factors other than the amount of catalyst addition are determined, so long-term and efficient imbibition grouting can be achieved by reasonable amount of catalyst addition. During construction, the gel time of silica sol under different catalyst additions should be measured by the inverted cup method according to the ambient temperature. It is recommended to set four-fifths of the gel time as the grouting construction time because the grouting material has good injectability and wettability at this time.

3.2. Characteristics of Imbibition Grouting under Multiple Factors

3.2.1. Effect of Catalyst and Temperature on Imbibition

The change of catalyst addition and temperature is the main factor affecting the gelation of silica sol. Figure 6a shows the change rule of the 1 mD artificial core on the silica sol imbibition curve and grout absorption under the influence of catalyst and temperature. The silica sol cannot be gelled without a catalyst, so long-term (3 days or more) absorption can be achieved, making it have the largest amount of grout absorption. However, as the single liquid of silica sol cannot form a solid gel, it cannot be directly applied to grouting construction. After adding the catalyst, the imbibition time of the silica sol was limited by the gel time, so that the amount of the grout absorbed was reduced to 1.85 g compared with that without the catalyst. However, the imbibition rate was higher than the case without the catalyst due to the dilution of the silica sol after adding the catalyst. As the temperature increased, the imbibition time of the silica sol gradually decreased, but the imbibition rate increased. The diffusion rate of particles increased with the increase in temperature, so the absorption rate increased significantly. At the same time, the increase in particle velocity made the number of collisions between particles increase, thus shortening the gel time (see Figure 6b).

The addition of a catalyst and the change of temperature will accelerate/slow down the gel time of the silica sol and then have a significant impact on the imbibition process. In the actual construction process, the ambient temperature is constant. In order to ensure a long imbibition time, the amount of catalyst can be adjusted so as to determine the appropriate gel time.

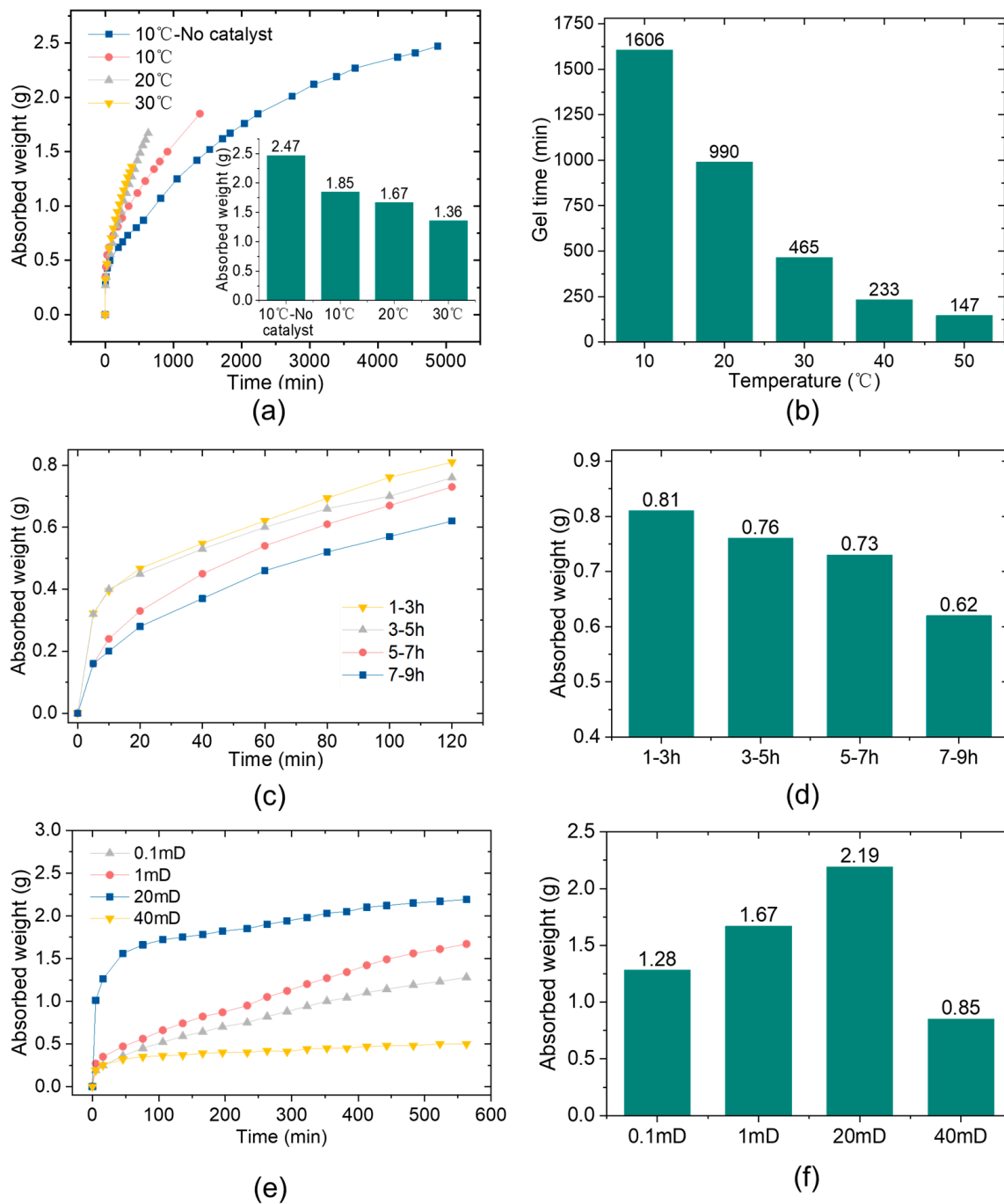


Figure 6. Imbibition characteristics of silica sol and artificial core. (a) Effect of catalyst and temperature on silica sol imbibition; (b) effect of temperature on silica sol-gel; (c) effect of the gel process on the imbibition curve; (d) effect of gel process on absorbed weight; (e) effect of rock mass permeability on imbibition curve; (f) effect of rock mass permeability on absorbed weight.

3.2.2. Effect of the Gel Process on Imbibition

The contact angle test in Section 3.1.3 showed that the presentation time of the imbibition characteristics of the silica sol with a ratio of 10:1 was 0–9 h. In allusion to the small change in the performance of the silica sol at the initial stage of gel, the imbibition curve of silica sol for every 2 h was tested from 1 h to characterize the influence of the gel process on imbibition. As shown in Figure 6c,d, the influence of the silica sol-gel on imbibition is represented by the imbibition rate and grout absorption. With the increase in the gel time, the core imbibition rate and the grout absorption gradually decreased. In the gelation

process of silica sol, the particle size of micelles increased gradually, and the injectability and wettability decreased gradually. The increasing particle size of micelles reduced the injectability of silica sol, and the percolation effect of silica particles in the micropores of the core was enhanced. At the same time, the reduction of grouting material wettability reduced the driving force for imbibition provided by capillary force. Due to the two factors, the imbibition process was inhibited, especially in the late stage of gelation. This is why the grout absorption from 7 h to 9 h was much lower than in other periods.

3.2.3. Effect of Rock Mass Permeability on Imbibition

For characterization of the effect of rock mass permeability on imbibition, the imbibition curves of low-permeability rock masses with four permeabilities of 0.1 mD, 1 mD, 20 mD, and 40 mD were tested as shown in Figure 6e,f.

As shown in Figure 6e, the imbibition curves of different samples showed two-stage distribution, namely, the severe imbibition stage and the stable imbibition stage. The severe imbibition stage occurred in the early stage of imbibition with the shortest duration, while the stable imbibition stage occurred in the middle and late periods of imbibition with the longest duration. For 0.1 mD and 1 mD samples, the grout absorption was less in the severe imbibition stage and more in the stable imbibition stage. For 20 mD and 40 mD samples, the grout absorption was more in the severe infiltration stage, and the proportion of grout absorption in this stage was more than 50%, while the grout absorption was less in the stable stage, at about 10%. Figure 6f shows the grout absorption of different cores. The grout absorption increased first and then decreased with the permeability; the maximum was 20 mD, and the minimum was 40 mD. Silica sol was able to be grouted into low-permeability artificial rock samples of all test permeability grades through spontaneous imbibition, i.e., artificial cores with a minimum permeability of 0.1 mD was able to be grouted by imbibition.

The macroscopic imbibition law of different core permeabilities is closely related to rock microstructure. Differences in the pore size distribution of rock samples, especially the pore characteristics of the nano-micro scale, have a remarkable influence on silica sol imbibition. The findings have shown that the T_2 curve of NMR can reflect the pore structure of the rock mass [45,46]. According to the principle of NMR [47,48], the pore size can be divided into three categories according to the relaxation time, namely, large pores ($T_2 > 100$ ms), medium pores (10 ms $< T_2 < 100$ ms), and small pores ($T_2 < 10$ ms). In order to reveal the absorption and permeability evolution mechanism of cores with different permeabilities, the T_2 distribution and pore structure characteristics of four artificial cores were tested by NMR, as shown in Figure 7.

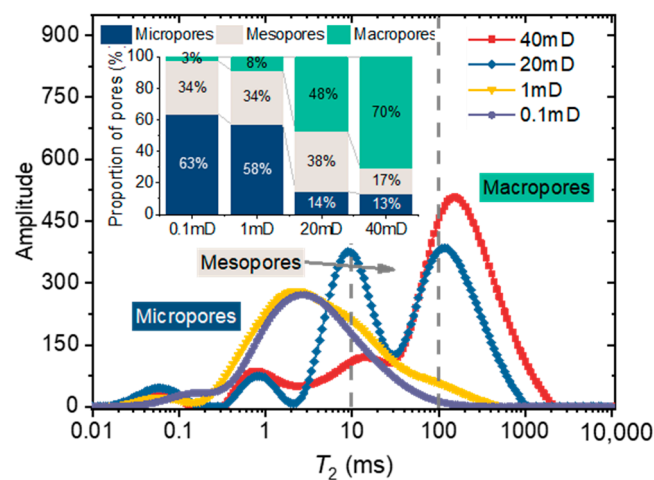


Figure 7. T_2 distribution law and pore structure characteristics of artificial cores.

Figure 7 shows that the 0.1 mD and 1 mD samples were dominated by minipore volumes (more than 50%), the 20 mD samples were dominated by mesopores and macropores, and the 40 mD samples were dominated by macropores. According to Section 3.1.2, the injectability of rock mass is related to the particle size and pore size of the grouting material. When the particle size of the grouting material is constant, the larger the macropores, the better the injectability of the rock mass. This shows that the injectability of artificial rock increases with the increase in permeability in the same gel time of silica sol. The capillary force as the internal driving force of imbibition is inversely proportional to the capillary radius, i.e., the smaller the pore, the greater the capillary force. In the range of 0.1–40 mD, the 0.1 mD sample with the largest proportion of minipores had the minimum injectability but the largest capillary force, while the 40 mD sample with the largest proportion of macropores had the maximum injectability but the minimum capillary force. The 20 mD rock core had strong injectability and capillary force at the same time, so the grout absorption was the largest. The above rules indicate that the injectability and capillary force of grouting material and rock mass will jointly affect the imbibition process of silica sol.

3.3. Pore Closure Characteristics of Rock Mass by Imbibition Grouting

After the silica sol is spontaneously imbibed and injected into the artificial rock, the nano-silica will inevitably fill in the micro-cracks of the artificial rock. This makes the artificial rock sample denser and less porous. At the same time, the imbibition process must be accompanied by complex processes such as adsorption, infiltration, and retention of silica sol, and the microscopic pore size distribution law of the rock mass will inevitably change accordingly. Under specific construction conditions, the amount of catalyst addition and the temperature are determined parameters, and the imbibition grouting is mainly affected by the permeability of the rock mass. Therefore, the vacuum saturation method and the nitrogen-adsorption method were used to characterize the pore sealing characteristics of low-permeability cores with different permeabilities before and after imbibition.

Table 6 shows the porosity change characteristics before and after imbibition, where the reduction in porosity of the sample was the filling amount of silica sol. After imbibition, each core had different levels of reduction in porosity. The pore sealing rate of the 20 mD core was 9.76%, which was the highest, while the pore sealing rate of the 40 mD core was 2.18%, which was the lowest. In the range of 0.1–40 mD, the reduction amount and rate of porosity were consistent with the variation of silica sol intake with permeability. This also shows that the gel formed by the spontaneous imbibition of silica sol into the core sealed the micro-pores of the rock mass, thereby reducing the porosity of the sample. The mechanism of pore sealing in rock mass was the same as that of imbibition.

Table 6. Porosity of rock mass before and after imbibition.

Rock Core/mD	Original Porosity/%	Final Porosity/%	Reduction /%	Reduction Rate/%
0.1	4.21	4.06	0.15	3.56
1	6.19	5.92	0.27	4.36
20	8.71	7.86	0.85	9.76
40	10.11	9.89	0.22	2.18

To reveal the pore sealing law of silica sol imbibition grouting at the microscopic level, appropriate amounts of rock blocks were taken from the top and bottom of the core for the microscopic pore size distribution test before and after imbibition (see Figure 8). The test results are shown in Figure 9.

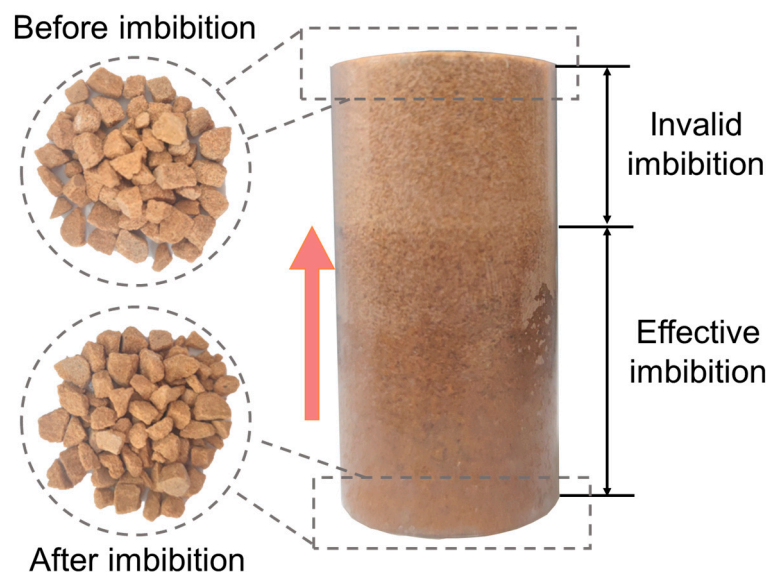


Figure 8. Schematic diagram of the sampling position.

The typical adsorption isotherm curve of artificial rock is shown in Figure 9a, and the porous structure can be qualitatively evaluated by the shape of the isotherm. According to the classification standard of specific surface area and the aperture test, the nitrogen adsorption isotherm of the original sandstone sample belongs to Type IV, so the Barrett–Joyner–Halenda (BJH) model [49,50] was used to obtain the pore volume and pore size distribution of the sample according to the desorption part of the isothermal adsorption desorption curve (Figure 9b). Utilizing this method, the pore size distribution law of 0.1–40 mD samples before and after imbibition were obtained, as shown in Figure 9c–f. On the whole, the pore size distribution of the four samples changed significantly after imbibition, and the maximum peak value of pore volume shifted to the left. This shows that the absorption of the silica sol changes the pore size distribution of the core.

According to the pore size distribution law of artificial cores, the change rule of average pore size and total pore volume before and after imbibition were obtained, as shown in Figure 9g–h. The overall law shows that both the average pore size and the total pore volume increased with the increase in permeability for 0.1–40 mD cores, indicating that the initial pore volume of the core increased with the increase in permeability. After imbibition, the pore volume of the rock mass decreased to varying degrees, and the reduction of the average pore diameter and total pore volume first increased and then decreased with the increase in permeability, and the reduction of the 20 mD core was the maximum, indicating that the microscopic laws of the average pore diameter and total pore volume before and after imbibition were consistent with the macroscopic pore sealing laws.

The imbibition of silica sol makes nano-silica particles adsorb and fill the micro-pores of rock mass, leading to the change of pore size distribution of rock mass. According to the pore classification standard of the International Union of Pure and Applied Chemistry [51] (IUPAC), the evolution laws of all kinds of pores before and after self-absorption and infiltration can be obtained. Since the proportion of pores below 2 nm is less than 1%, the pores below 2 nm are not taken into account alone. The pores are divided into >50 nm pores and <50 nm pores. On this basis, the microscopic pore structure distribution characteristics of each core before and after imbibition are shown in Table 7.

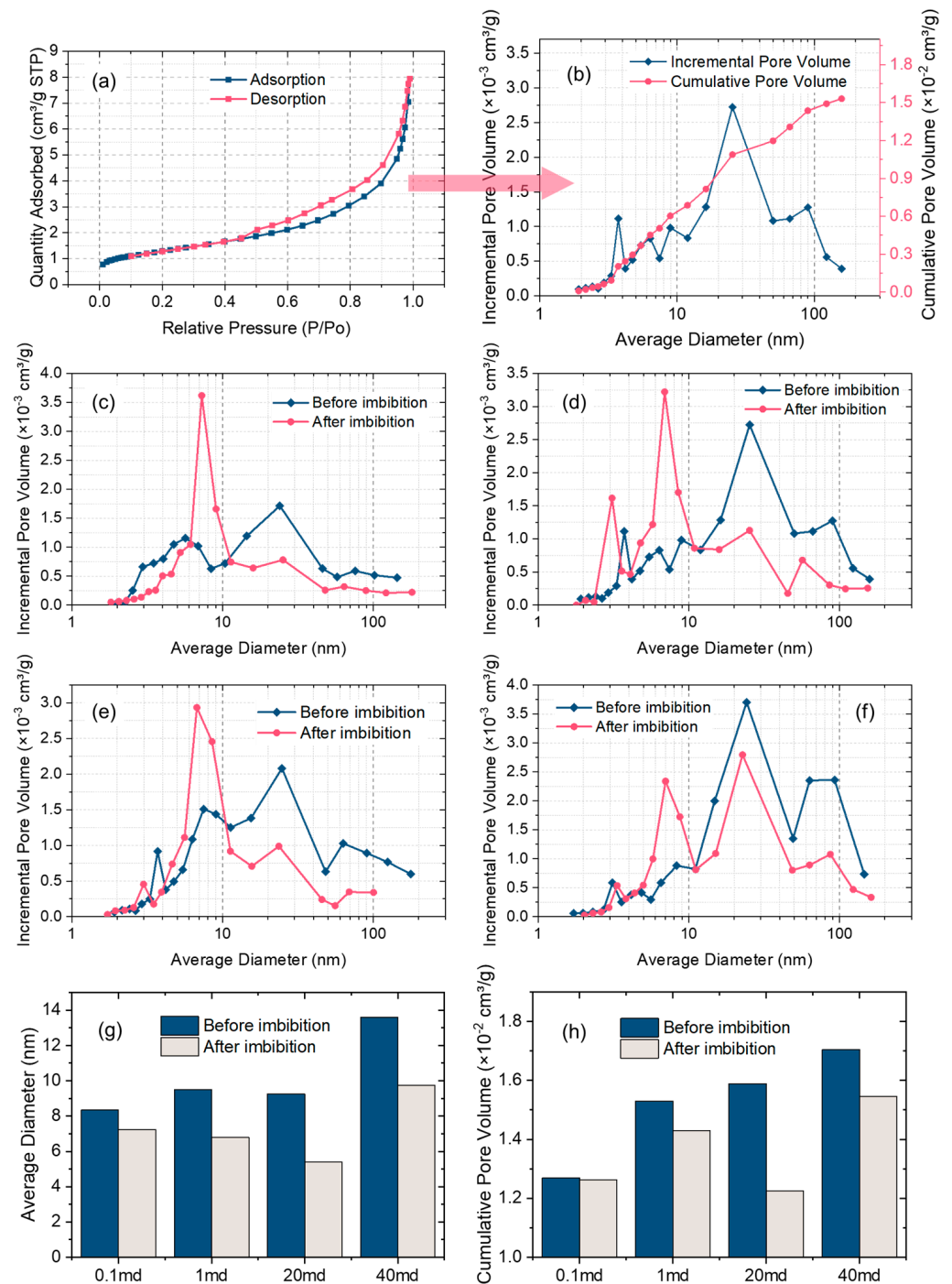


Figure 9. Micropore distribution characteristics of rock mass before and after imbibition. (a) Isothermal adsorption–desorption curve of artificial core; (b) pore size distribution law of artificial core; (c) pore size distribution of 0.1 mD core before and after imbibition; (d) pore size distribution of 1 mD core before and after imbibition; (e) pore size distribution of 20 mD core before and after imbibition; (f) pore size distribution of 40 mD core before and after imbibition; (g) variation law of average pore diameter before and after imbibition; (h) variation law of cumulative pore volume before and after imbibition.

Table 7. Micro distribution characteristics of pores before and after imbibition.

Rock Cores		>50 nm		<50 nm	
		Pore Volume ($\times 10^3 \text{ cm}^3/\text{g}$)	Percentage (%)	Pore Volume ($\times 10^3 \text{ cm}^3/\text{g}$)	Percentage (%)
0.1 mD	Before imbibition	2.07	16.28	10.62	83.72
	After imbibition	1.01	7.96	11.63	92.04
1 mD	Before imbibition	4.43	28.92	10.88	71.08
	After imbibition	1.49	10.4	12.8	89.6
20 mD	Before imbibition	3.92	24.66	11.97	75.34
	After imbibition	1.08	8.85	11.17	91.15
40 mD	Before imbibition	5.45	31.97	11.6	68.03
	After imbibition	2.77	17.93	12.69	82.07

Before imbibition, the pore proportion of >50 nm increased with the increase in permeability for the core of 0.1–40 mD, indicating that the pore volume of rock mass increased gradually. After imbibition, the porosity of >50 nm decreased, and the porosity of <50 nm decreased significantly. Moreover, the main pore size after imbibition was less than 10 nm, i.e., about 7 nm. On the one hand, the spontaneous imbibition of silica sol into the rock mass will form gel to block the pores, making the pore volume of >50 nm significantly reduced. In addition, after nano-silica enters the pore throat, some nano-silica particles will be adsorbed and retained on the surface of the pore throat, and the particles with particle sizes smaller than the pore throat size will be screened out of the pore throat because of the complex bending of the pore throat channel and the large specific surface area and high surface energy of silica sol. This makes a large number of silica particles adsorbed in the micropore throat. This part of silica particles reduces the pore volume and forms a large number of segmented micro-void space smaller than the size of silica particles, resulting in the pore volume peak (smaller than the size of nano-silica) of about 7 nm after imbibition. And the more developed the nano-scale pores (see Figure 7), the larger the pore volume peak of about 7 nm after imbibition, for example, the peak value of 0.1 mD was higher than that of the 40 mD core, indicating that the adsorption and retention of nano-silica are related to nano-scale micro-pores.

The initial median particle size of the silica sol is small, and both d_{95} and $3d_{95}$ are in the nanometer-scale. Compared with conventional cement grout, and superfine cement grout [42,52], the particle size of silica sol has obvious advantages. In this study, further, the silica sol was able to be grouted into 0.1–40 mD rock cores by spontaneous imbibition. This further verifies the feasibility of silica sol imbibition grouting to seal low-permeability rock mass. Compared with high-pressure grouting, imbibition greatly reduces the injectable permeability of silica sol as low as 0.1 mD (in this experiment), which makes up for the deficiency of high-pressure grouting on the injectability of low-permeability rock mass to some extent. This shows that the silica sol imbibition can meet the engineering requirements for the sealing and reinforcement of nano-micropores in low-permeability argillaceous rock mass. At the same time, in the aspect of silica sol grouting to plug nanoscale micro-cracks in the rock mass, Pan's research shows that the minimum theoretically injectable crack width of silica sol is 186 nm [25]. According to Chai's research, the minimum injectable pore width of silica sol is as low as 20 nm [53]. The research in this paper found that the silica sol also has a certain injectability for smaller-width cracks, and the crack width was as low as 7 nm. The natural mudstone is mostly in a dry or unsaturated water state, so the interface between silica sol and mudstone has good wettability and strong affinity, with obvious potential for imbibition. When the project is implemented, the mutual imbibition can be fully utilized. In view of the construction operability, the silica sol grouting of low-permeability rock mass should be carried out by means of low-pressure slow seepage or high-low-pressure grouting. Under the condition of keeping low pressure for a long time, the capillary force between silica sol and rock mass spontaneously imbibes into the

micro pores of rock mass and thus the sealing reinforcement effect of low-permeability fractured rock mass is further improved.

4. Conclusions

In this paper, the regularities and mechanism of grouting and pore sealing of low-permeability rock mass under silica sol imbibition were preliminarily studied based on the gelling properties of silica sol, core pore structure, imbibition law and pore sealing characteristics, and so on. Silica sol can seal pores of low-permeability cores by imbibition. Through the development of nanoscale materials, we expect to fundamentally solve the problem of grouting and anti-seepage in rock masses. The following conclusions are drawn:

- (1) Adding a strong electrolyte-type catalyst can adjust the gel time of the silica sol, and the catalyst ratio was distributed exponentially with the gel time. The particle size growth during the gelation process of silica sol resulted in a significant change in the injectability and wettability of the silica sol. The deterioration inflection points of injectability and wettability appeared at 10 h and 9 h, respectively.
- (2) The catalyst and temperature can prolong or shorten the overall imbibition time by affecting the gel time. The injectability and capillary force of grouting material and rock mass will jointly affect the imbibition process of silica sol in the permeability range of 0.1–40 mD.
- (3) The imbibition of silica sol changes the pore size distribution of the core, the pore volume >50 nm decreased, and the pore volume <50 nm increased. The complex process of nano silica sol filling, adsorption, percolation, retention, and other complex processes to the micropores of the rock mass reduced the size of the main pores of the rock mass after imbibition to about 7 nm.
- (4) Limitations of research and future work: In this article, artificial low-permeability rocks were used instead of muddy rock masses to conduct experiments, without considering the impact of changes in physical properties such as rock swelling and mud formation after mud absorption on the infiltration of muddy rock masses.

Author Contributions: Conceptualization, Y.Z.; Methodology, Z.X. and N.Z.; Software, Z.X.; Validation, Y.Z. and J.D.; Formal analysis, Z.X. and N.Z.; Investigation, J.D.; Resources, Y.Z.; Data curation, N.Z.; Writing—original draft, Y.Z. and Z.X.; Writing—review & editing, Y.Z., Z.X. and N.Z.; Visualization, Z.X. and J.D.; Supervision, N.Z.; Funding acquisition, Y.Z. All authors have read and agreed to the published version of the manuscript.

Funding: This work was supported by National Natural Science Foundation of China (Nos. 52034007, 52274146, and 52108365) and the Fundamental Research Funds for the Central Universities (No. 2024QN11003).

Data Availability Statement: The original contributions presented in the study are included in the article.

Acknowledgments: The authors are grateful to the experimenters at the State Key Laboratory of Coal Resources and Safe Mining for their assistance during the experiment.

Conflicts of Interest: The authors declare no conflict of interest.

References

1. Jin, Y.; Han, L.; Guo, H.; Yang, S.; Su, S.; Liu, Z.; Wang, S. Mechanical and macro-microscopic failure characteristics of grouted mudstone considering grout dehydration effect. *Eng. Fail. Anal.* **2022**, *142*, 106662. [[CrossRef](#)]
2. Tian, H.; Chen, W.; Tan, X.; Shu, X. Failure of rigid support and yielding support solution in large deformation tunnels: A case study. *Eng. Fail. Anal.* **2022**, *140*, 106598. [[CrossRef](#)]
3. Koralegedara, N.H.; Maynard, J.B. Chemical, mineralogical and textural properties of the kope formation mudstones: How they affect its durability. *Eng. Geol.* **2017**, *228*, 312–322. [[CrossRef](#)]
4. Zhao, Y.; Ren, S.; Jiang, D.; Liu, R.; Wu, J.; Jiang, X. Influence of wetting-drying cycles on the pore structure and mechanical properties of mudstone from simian mountain. *Constr. Build. Mater.* **2018**, *191*, 923–931. [[CrossRef](#)]
5. Zhu, Q.; Li, T.; Wang, B.; Li, C.; Ran, J.; Zhang, H. A case study on the deformation and failure mechanism of a soft rock mining roadway in the Xin’Shang’Hai No. 1 coal mine, China. *Eng. Fail. Anal.* **2023**, *146*, 107136. [[CrossRef](#)]

6. Liu, J.; Xu, Q.; Wang, S.; Subramanian, S.S.; Wang, L.; Qi, X. Formation and chemo-mechanical characteristics of weak clay interlayers between alternative mudstone and sandstone sequence of gently inclined landslides in Nanjiang, SW China. *Bull. Eng. Geol. Environ.* **2020**, *79*, 4701–4715. [[CrossRef](#)]
7. Wang, L.L.; Bornert, M.; Héripré, E.; Chanchole, S.; Pouya, A.; Halphen, B. The mechanisms of deformation and damage of mudstones: A micro-scale study combining ESEM and DIC. *Rock Mech. Rock Eng.* **2015**, *48*, 1913–1926. [[CrossRef](#)]
8. Liu, B.; Yang, H.; Karekal, S. Effect of water content on argillization of mudstone during the tunnelling process. *Rock Mech. Rock Eng.* **2020**, *53*, 799–813. [[CrossRef](#)]
9. Zhao, C.; Li, Y.; Liu, G.; Meng, X. Mechanism analysis and control technology of surrounding rock failure in deep soft rock roadway. *Eng. Fail. Anal.* **2020**, *115*, 104611. [[CrossRef](#)]
10. Sandbak, L.A.; Rai, A.R. Ground support strategies at the turquoise ridge joint venture, Nevada. *Rock Mech. Rock Eng.* **2013**, *46*, 437–454. [[CrossRef](#)]
11. Xiong, H. *Geotechnical Engineering Chemistry*; Science Press: Beijing, China, 2009.
12. Kim, M.; Corapcioglu, M. Gel barrier formation in unsaturated porous media. *J. Contam. Hydrol.* **2002**, *56*, 75–98. [[CrossRef](#)] [[PubMed](#)]
13. Axelsson, M. Mechanical tests on a new non-cementitious grout, silica sol: A laboratory study of the material characteristics. *Tunn. Undergr. Space Technol.* **2006**, *21*, 554–560. [[CrossRef](#)]
14. Kutzner, C. *Grouting of Rock and Soil*; Balkema: Rotterdam, The Netherlands, 1996.
15. Liu, C. Development of Modified Silica Sol Grouting Material and Its Sand Grouting Simulation. Master's Thesis, Tianjin University, Tianjin, China, 2018.
16. Sögaard, C.; Funehag, J.; Abbas, Z. Silica sol as grouting material: A physio-chemical analysis. *Nano Converg.* **2018**, *5*, 6. [[CrossRef](#)] [[PubMed](#)]
17. Zhang, M.Q.; Feng, P. *Grouting Technology of Underground Engineering*; Science Press: Beijing, China, 2008.
18. Funehag, J.; Gustafson, G. Design of grouting with silica sol in hard rock—New methods for calculation of penetration length, Part I. *Tunn. Undergr. Space Technol.* **2008**, *23*, 1–8. [[CrossRef](#)]
19. Funehag, J.; Gustafson, G. Design of grouting with silica sol in hard rock—New design criteria tested in the field, Part II. *Tunn. Undergr. Space Technol.* **2008**, *23*, 9–17. [[CrossRef](#)]
20. Butrón, C.; Gustafson, G.; Fransson, Å.; Funehag, J. Drip sealing of tunnels in hard rock: A new concept for the design and evaluation of permeation grouting. *Tunn. Undergr. Space Technol.* **2010**, *25*, 114–121. [[CrossRef](#)]
21. Wang, Q.C.; Li, H.; Zhu, N. Research on water plugging with nanoscale grouting material and high-property concrete in slope shaft. *Coal Min. Technol.* **2013**, *18*, 97–108. [[CrossRef](#)]
22. Holter, K.; Hognestad, H. Modern pre-injection in underground construction with rapid-setting microcements and colloidal silica—Applications in conventional and TBM-tunnelling. *Geomech. Tunn.* **2012**, *5*, 49–56. [[CrossRef](#)]
23. Date, K.; Narita, N.; Yokota, Y.; Takuji, Y.; Sakamaki, S.; Kashiwaya, M. Pre-grouting and chemical injection for preserving groundwater environment and safe tunnelling. In *World Tunnel Congress, Underground: The Way to the Future*; Taylor & Francis Group: Geneva, Switzerland, 2013.
24. Pan, D.; Hong, K.; Fu, H.; Zhou, J.; Zhang, N.; Lu, G. Influence characteristics and mechanism of fragmental size of broken coal mass on the injection regularity of silica sol grouting. *Constr. Build. Mater.* **2020**, *269*, 121251. [[CrossRef](#)]
25. Pan, D.J. *Study on Permeability Law of Silica Sol Grouting and Long-Term Consolidation Stability of Loose Coal*; China University of Mining and Technology: Beijing, China, 2018.
26. Guo, F.; Xie, Z.; Zhang, N.; Zhang, C.; Guo, H.; Cui, G.; Xiang, Z. Study on the Pore-throat structure characterization and nano grouting law of the Low-permeability mudstone based on NMR-RSM methods. *Constr. Build. Mater.* **2022**, *342*, 127913. [[CrossRef](#)]
27. Sun, X.T.; Zhou, H.W.; Xue, D.J. Experimental study of spontaneous imbibition of low-permeability coal based on NMR. *J. China Univ. Min. Technol.* **2021**, *50*, 804–812. [[CrossRef](#)]
28. Shun, L.; Jun, N.; Xianli, W.; Xiong, L.; Zhaoqin, H.; Desheng, Z.; Pengju, R. A dual-porous and dual-permeable media model for imbibition in tight sandstone reservoirs. *J. Pet. Sci. Eng.* **2020**, *194*, 107477. [[CrossRef](#)]
29. Qiu, R.D.; Gu, C.Y.; Xue, P.Y.; Xu, D.X.; Gu, M. Imbibition characteristics of sandstone cores with different permeabilities in nanofluids. *Pet. Explor. Dev.* **2022**, *49*, 374–381. [[CrossRef](#)]
30. Su, Z.; Wang, Z.; Zhang, D.; Wei, T. Study on rheological behavior and surface properties of epoxy resin chemical grouting material considering time variation. *Materials* **2019**, *12*, 3277. [[CrossRef](#)]
31. Gong, J. *Research on Osmotic Dynamics of Epoxy Slurry for Low-Permeability Bad Geological Body*; Changjiang River Scientific Research Institute: Wuhan, China, 2018.
32. Tamar, Y.; Sasson, Y. Examination of the regime controlling sol–gel based colloidal silica aggregation. *J. Non-Cryst. Solids* **2013**, *380*, 35–41. [[CrossRef](#)]
33. Simonsson, I.; Sögaard, C.; Rambaran, M.; Abbas, Z. The specific co-ion effect on gelling and surface charging of silica nanoparticles: Speculation or reality? *Colloid Surf. A* **2018**, *559*, 334–341. [[CrossRef](#)]
34. Metin, C.O.; Bonnacaze, R.T.; Lake, L.W.; Miranda, C.R.; Nguyen, Q.P. Aggregation kinetics and shear rheology of aqueous silica suspensions. *Appl. Nanosci.* **2014**, *4*, 169–178. [[CrossRef](#)]
35. Metin, C.O.; Lake, L.W.; Miranda, C.R.; Nguyen, Q.P. Stability of aqueous silica nanoparticle dispersions. *J. Nanoparticle Res.* **2011**, *13*, 839–850. [[CrossRef](#)]

36. Yang, K. Diagenesis of Carboniferous Batamayineshan Formation Volcanic Reservoir in Eastern Junggar Basin. Ph.D. Thesis, Jilin University, Changchun, China, 2019.
37. Holtta, P.; Lahtinen, M.; Hakanen, M.; Lehto, J.; Juhola, P. The influence of groundwater on the stability of silica colloids. *Mater. Res. Soc.* **2009**, *1193*, 437. [[CrossRef](#)]
38. Pedrotti, M.; Wong, C.; El Mountassir, G.; Lunn, R. An analytical model for the control of silica grout penetration in natural groundwater systems. *Tunn. Undergr. Space Technol.* **2017**, *70*, 105–113. [[CrossRef](#)]
39. He, Z.; Wang, L.G.; Liu, B. *Theory and Application of Grouting in Rock Mass*; Geological Press: Beijing, China, 2006.
40. Cui, J.J.; Cui, X.Q. *Grouting Technology of Tunnel and Underground Engineering*; China Construction Industry Press: Beijing, China, 2011.
41. Pan, D.; Zhang, N.; Xie, Z.; Feng, X.; Kong, Y. Laboratory Testing of Silica Sol Grout in Coal Measure Mudstones. *Materials* **2016**, *9*, 940. [[CrossRef](#)] [[PubMed](#)]
42. Zhang, C. Study on the Diffusion Law of Nano Slurry Based on Three-Dimensional Characterization of Coal-Measure Mudstone Pores and Fractures. Master's Thesis, China University of Mining and Technology, Beijing, China, 2019.
43. Fu, T.-F.; Xu, T.; Heap, M.J.; Meredith, P.G.; Yang, T.-H.; Mitchell, T.M.; Nara, Y. Analysis of capillary water imbibition in sandstone via a combination of nuclear magnetic resonance imaging and numerical DEM modeling. *Eng. Geol.* **2021**, *285*, 106070. [[CrossRef](#)]
44. Xu, L.; Li, Q.; Myers, M.; Tan, Y. Effects of bedding direction on brine imbibition in Lower Shaximiao tight sandstone: An NMR analysis. *J. Pet. Sci. Eng.* **2022**, *210*, 110006. [[CrossRef](#)]
45. Zhou, K.; Liu, T.; Hu, Z. Exploration of damage evolution in marble due to lateral unloading using nuclear magnetic resonance. *Eng. Geol.* **2018**, *244*, 75–85. [[CrossRef](#)]
46. Golsanami, N.; Sun, J.; Zhang, Z. A review on the applications of the nuclear magnetic resonance (NMR) technology for investigating fractures. *J. Appl. Geophys.* **2016**, *133*, 30–38. [[CrossRef](#)]
47. Zhai, C.; Wu, S.; Liu, S.; Qin, L.; Xu, J. Experimental study on coal pore structure deterioration under freeze–thaw cycles. *Environ. Earth Sci.* **2017**, *76*, 507. [[CrossRef](#)]
48. Cai, Y.; Liu, D.; Pan, Z.; Yao, Y.; Li, J.; Qiu, Y. Petrophysical characterization of Chinese coal cores with heat treatment by nuclear magnetic resonance. *Fuel* **2013**, *108*, 292–302. [[CrossRef](#)]
49. Barrett, E.P.; Joyner, L.G.; Halenda, P.P. The determination of pore volume and area distributions in porous substances. I. Computations from nitrogen isotherms. *J. Am. Chem. Soc.* **1951**, *73*, 373–380. [[CrossRef](#)]
50. Yao, Y.; Liu, D.; Yan, T. Geological and hydrogeological controls on the accumulation of coalbed methane in the Weibei field, southeastern Ordos Basin. *Int. J. Coal Geol.* **2014**, *121*, 148–159. [[CrossRef](#)]
51. Thommes, M.; Kaneko, K.; Neimark, A.V.; Olivier, J.P.; Rodriguez-Reinoso, F.; Rouquerol, J.; Sing, K.S.W. Physisorption of gases, with special reference to the evaluation of surface area and pore size distribution. *Pure Appl. Chem.* **2015**, *87*, 1051–1069. [[CrossRef](#)]
52. Zheng, K.; Liu, Y.; Huang, W.; Zhou, J.; Cui, D. Reverse filling cementitious materials based on dense packing: The concept and application. *Powder Technol.* **2020**, *359*, 152–160. [[CrossRef](#)]
53. Chai, Z.; Liu, X.; Yang, P.; Guo, R.; Yang, Z. Experimental study on physical properties of silica soil and grouting modified mudstone. *Chin. J. Rock Mech. Eng.* **2021**, *40* (Suppl. S1), 2682–2691.

Disclaimer/Publisher's Note: The statements, opinions and data contained in all publications are solely those of the individual author(s) and contributor(s) and not of MDPI and/or the editor(s). MDPI and/or the editor(s) disclaim responsibility for any injury to people or property resulting from any ideas, methods, instructions or products referred to in the content.